JOURNAL OF BIOMOLECULAR STRUCTURE AND DYNAMICS
2024, VOL. 42, NO. 4, 1795–1811
https://doi.org/10.1080/07391102.2023.2202279

Preparation and evaluation *in vitro* release of sodium alginate/chitosan polyelectrolyte microparticles containing rifampicin and theoretical study using DFT methods

Nadia A. Hussein Al-Assady[a], Hussain A. Badran[b], Sarah A. Kamil[a] and Ryadh Ch. Abo-Alhal[b]

[a]Department of Chemistry, College of Education for Pure Science, University of Basrah, Basrah, Iraq; [b]Department of Physics, College of Education for Pure Science, University of Basrah, Basrah, Iraq

Communicated by Ramaswamy H. Sarma

ABSTRACT

In this work, rifampicin-loaded sodium alginate/chitosan polyelectrolyte microparticles were prepared by the ionotropic gelation technique using $CaCl_2$ as a cross-linking agent. The influence of different sodium alginate and chitosan concentrations on particle size, surface properties, and *in vitro* release behavior was studied. An infrared spectroscopy investigation verified the lack of any drug–polymer interaction. The microparticles prepared using (30, 50) mg of sodium alginate were spherical while when using 75 mg of sodium alginate, vesicles with round heads and tapered tails were formed. The results showed that the microparticle diameters were between (11.872–35.3645) μm. The amount of rifampicin released and the kinetics of drug release from microparticles were studied, and the results showed that by increasing the concentration of the polymer, the release of the rifampicin from the microparticles decreased. The findings showed that rifampicin release followed zero-order kinetics and that drug release from these particles is frequently influenced by diffusion. The electronic structure and characteristics of the conjugated polymers (sodium alginate/Chitosan) were examined using density functional theory (DFT) and PM3 calculations with Gaussian 9, using the B3LYP, and electronic structure calculations using 6–311 G (d,p). The HOMO and LUMO energy levels are determined as the HOMO's maximum and the LUMO's minimum, respectively.

ARTICLE HISTORY
Received 15 October 2022
Accepted 8 April 2023

KEYWORDS
DFT; HOMO & LUMO; rifampicin; sodium alginate/chitosan polyelectrolyte

1. Introduction

With the progress in the field of biotechnology and combinatorial chemistry, and due to the problems associated with many new medicines such as low solubility rate, high efficacy, and poor stability of many of them, the most effective and targeted treatments are currently being created (Patel et al.,2016, Sabzini et al., 2023, Maryam et al., 2022). The means of medicine delivery can affect the effectiveness and marketability of the medicine as much as the drug itself (Fatemeh et al., 2022, Narges et al., 2022). Therefore, it has become necessary to deliver therapeutic agents to the target tissue in an ideal quantity and the correct period, with less toxicity and fewer side effects. There are different methods for delivering the therapeutic substance to the target site in constant controlled release patterns (Sohrab et al., 2022) and one of these methods is the use of microparticles as drug carriers (Mari et al., 2014). Microparticles are minuscule spherical particles that range in size from (1–1000 m) and are made up of one or more immiscible polymers with drug particles scattered throughout (Vos et al.,2014). Chemotherapy, cardiovascular illness, hormone treatment, therapeutic proton delivery, and vaccine research are just a few uses of microparticles in controlled drug-release systems (Patra et al., 2018).

Electrostatic interaction between two oppositely charged polyelectrolyte solutions produces sodium alginate/chitosan polyelectrolyte (SA/CH PE) (Kumar et al., 2018). Many investigations have been conducted on the use of (SA/CH PE) in medicine (Hamid et al., 2019; Buriuli &Verma 2017). Based on the electrostatic interactions between carboxylate alginate groups (COO–) and ammonium chitosan groups (NH_3^+), chitosan, a polysaccharide formed by alkaline deacetylation of chitin, has been used to support alginate microparticles. (SA/CH PE) erode slowly in phosphate buffer and this behavior leads to suppression of the initial release of drugs occurring in uncoated microparticles (Meng et al., 2010). These microparticles are usually made in two stages, with premade alginate microparticles being recovered and then coated with chitosan (Luo &Wang, 2014). Chitosan coating of low-sizing alginate microparticles is a cumbersome operation, thus doing it during the procedure using a simple approach might be a viable option (Moghimi et al., 2016). It would also aid in the retention of encapsulation during emulsification.

Rifampicin ($C_{43}H_{58}N_4O_{12}$) Figure 1 is an antibiotic with activity against many types of bacteria that cause tuberculosis, leprosy, meningitis, and brucellosis. Common side effects include nausea, vomiting, loss of appetite, and diarrhea. It has the most serious side effects, including

CONTACT Hussain A. Badran hussain_badran@yahoo.com

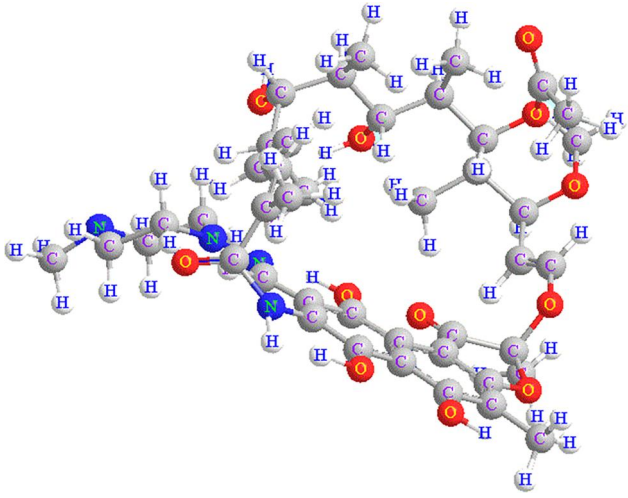

Figure 1. Two-dimensional structure of rifampicin.

hepatotoxicity, enzyme absorption, and drug interactions with other drugs (Gierszewska et al., 2018).

Rifampicin (RIF) is a class II drug in the Biopharmaceutical Classification System. The drugs of this class exhibit poor water solubility, high permeability, and low bioavailability after oral administration due to their poor water solubility (Sharma et al., 2021). In numerous studies, polymeric microparticles have been shown to be a targeted delivery system for treating and releasing rifampicin for therapy lung infections, because of its ability to stick to the lungs, can delay the release of rifampicin, protect the patient by preventing the drug from being degraded by enzyme hydrolysis, and prolonging the drug's life (drug retention in the lungs), in addition to reducing side effects. Microparticle polymeric drug delivery systems offer notable advantages to specialists and patients, such as choice of dosage form and method of drug delivery (oral tablets, parenteral injections) microparticles can be injected using hypodermic injection needles, unlike the surgical methods used for sustained-release implants particles (10–30 μm) are used for the therapeutic purpose by directly injecting in the veins that are linked to the targeted organ or tissue (Mazini et al., 2021).

For drug discovery design and logical synthesis, computational chemistry can be employed as a starting point (Pyta et al., 2012; Sliwoski et al., 2014). As a result, using computational chemistry in the design and rational synthesis of pharmaceuticals is a valuable tool for estimating the molecular interactions that occur in the drug delivery system, as well as predicting and selecting the most appropriate delivery method. Moreover, computational simulations have recently emerged for use in drug delivery systems, mainly in the controlled delivery of anti-cancer and anti-TB drugs. The major goal of this research is to discover the best method for the addition of non-covalent drugs to polymers by obtaining structural and electrical characteristics (Atif et al., 2014; Bai et al., 2019; Bazyari et al., 2020; 2021; Shariatinia & Mazloom, 2019; Hussein et al., 2014; Juarez et al., 2017; Narra et al., 2012). The aim of this study is to prepare a very tiny pharmaceutical (microparticles)form, using biopolymeric sodium alginate to be one of the first steps in microencapsulation technology application and covering sodium alginate microparticles with chitosan to control drug release of RIF drug, improving drug dissolution, reducing side effects, increasing efficacy, and enhancing bioavailability and stability. This study will investigate the potential of sodium alginate with chitosan for preparing microparticles with desired properties and application potentials.

Table 1. Design of the various formulas Rifampicin microparticles.

Batch code	RIF (mg)	SA (mg)	H_2O (ml)	CH (mg)	acetic acid 2% v/v
RM1	100	30	10	30	30
RM2	100	50	10	30	30
RM3	100	75	10	30	30
RM4	100	30	10	60	30
RM5	100	30	10	90	30

2. Materials and methods

Rifampicin was provided by (NDI Company in Iraq). Sodium Alginate) SA (was provided by (Fluka co.-Switzerland). Chitosan was supplied by (Sigma-Aldrich). Dialysis membrane (12,000–14,000) molecular weight cut off was ordered from Spectrum Laboratories Inc., USA weight cut off of (12,000–14,000) was ordered.

2.1. Preparation of sodium alginate/chitosan polyelectrolyte microparticles

The microparticles of SA were prepared using the inotropic gelation technique, which involved dissolving different weights of SA in 10 ml of distilled water for 1 h at a temperature of 50 °C. Additionally, 100 mg of RIF was dissolved in 2 ml of methanol and then mixed with the SA solution. (i.e., a carrier solution).In another baker, chitosan solutions were prepared by dissolution of the required amount of chitosan in 30 ml of freshly prepared 2% v/v acetic acid solution and dissolved using a magnetic stirrer at 150 rotations per minute (rpm) for 3 h, its pH value was adjusted to 5.5 with 0.1 M acetate buffer. Then, 0.3 g $CaCl_2$ was added and dissolves in the chitosan solution (i.e., a cross-linking solution). The weights of SA, CH, RIF, and the coding of prepared formulas are presented in Table 1. The carrier solution was placed through a medical syringe into a beaker containing cross linking agent solution and stirred continuously with a magnetic mixer for 0.5 h before being filtered, washed with isopropyl alcohol, and dried at 25 degrees Celsius (Scheme 1).

2.2. Characterization of microparticles

2.2.1. Surface morphology study

The optical microscope (Optka microscope B-'290 Series) and Leica ICC50 HD Microscope Camera were used to measure the diameter of RIF microparticles. Dry microparticles were suspended in distilled water (10 ml). The suspension was stirred for 5 s. A small drop of suspension obtained was placed on a clean glass slide. The slide containing RIF microparticles was fixed on the microscope stage. The diameter of (400 particles) was determined using a calibrated ocular micrometer.

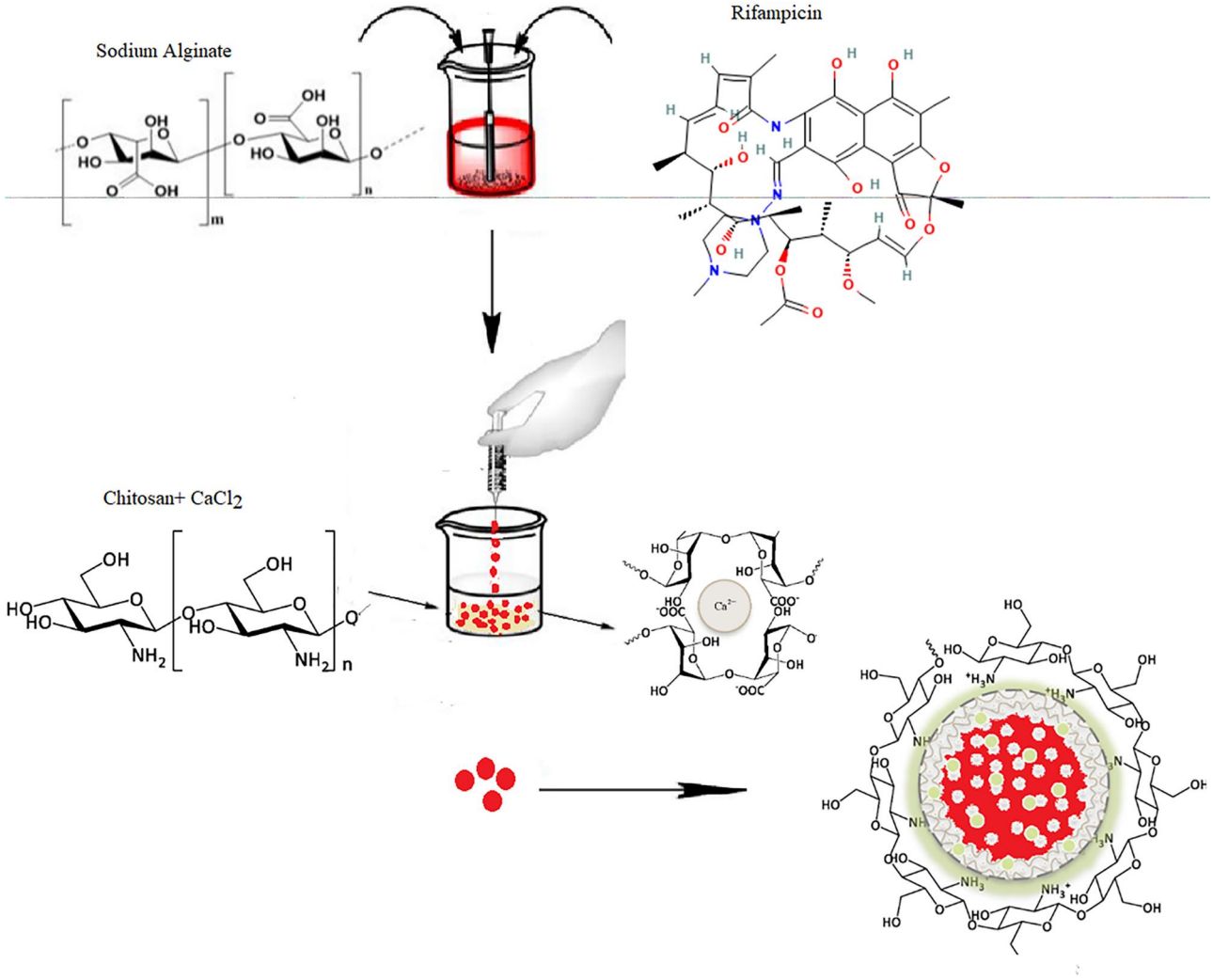

Scheme 1. Sodium alginate/chitosan polyelectrolyte microparticles preparation in two steps: (I) carrier solution (II) cross-linking solution, and (III) polyelectrolyte complexation.

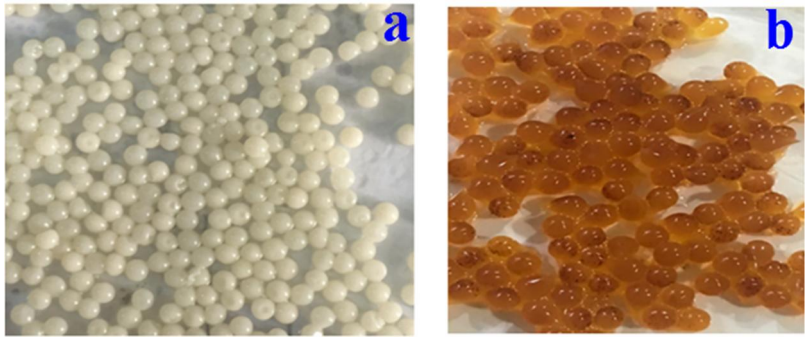

Figure 2. Photograph of sodium alginate/chitosan microparticles using normal camera images with mm scale (a) without RIF, (b) with RIF.

2.2.2. Determination of RIF loading efficiency

10 mg of RIF loaded microparticles from each batch were dissolved in 100 ml of phosphate buffer solution of pH 7.2 by shaking on a mechanical shaker for 24 h. After filtering using Whatmann filter paper, the solution was ready for use. An aliquot following suitable dilution was assayed UV-spectrophotometer, the samples were examined spectrophotometrically at λ_{max} 475 nm. The following equation was used in order to assess the RIF loading efficiency.

$$\text{RIF loding efficiency}\% = \frac{\text{Experimental RIF Content}}{\text{Theoretical RIF Content}} \times 100\% \quad (1)$$

2.2.3. Investigation of FT-IR spectroscopy

At room temperature, record the infrared spectra in the range (400–4000) cm^{-1} of the SA, RIF, BSA, and RIF loaded microparticles in the shape of tablets KBr.

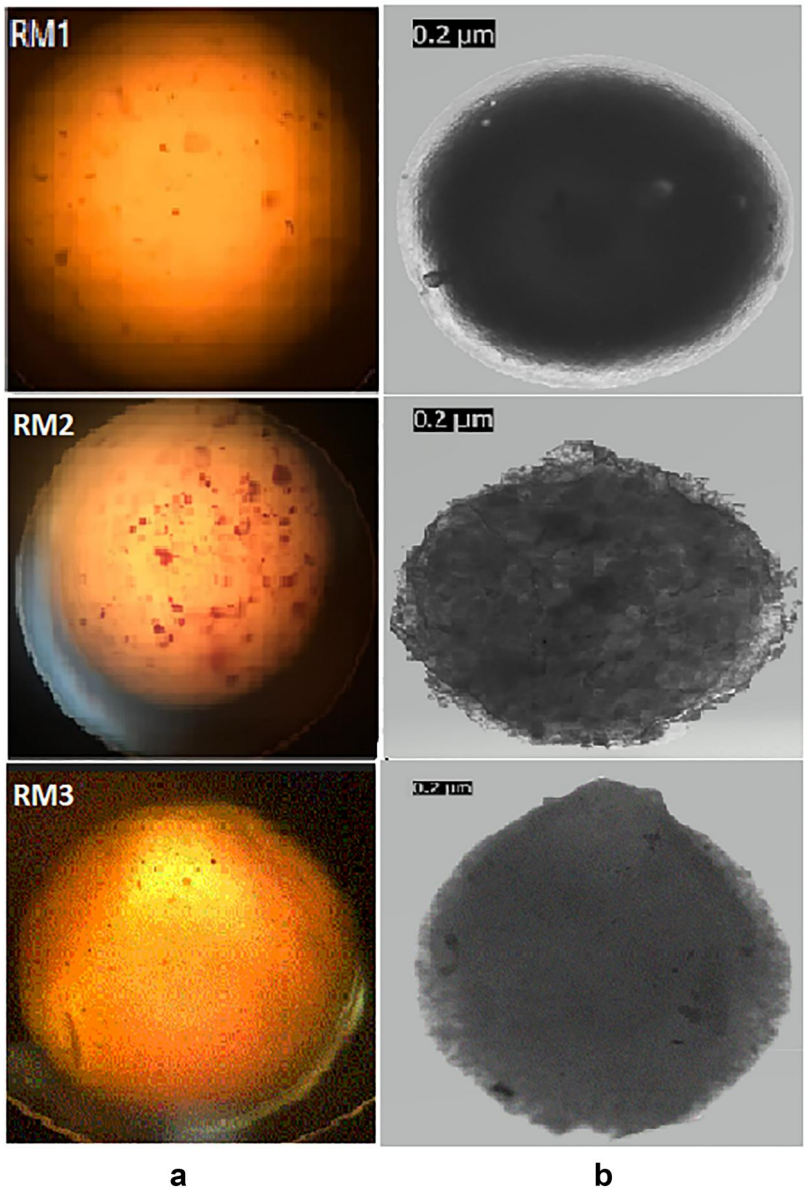

Figure 3. Photographic images of sodium alginate/chitosan loaded RIF. (a) Optical microscopy image (×40 magnification), (b) images were captured with a Leica ICC50 HD microscope camera. Each value is the mean of three independent measurements.

Table 2. Diameters of microparticles estimated in microns and the number of microparticles corresponding to each average dimension for formulation RM1.

Particle diameter (µm)	Mean particle diameter (*d*) (µm)	Number of fields examined (*n*)	(nd)
3.33–6.66	5	0	0
6.66–8.4	7.53	13	65
8.4–10.6	9.5	44	331.32
10.6–12.6	11.6	104	988
12.6–14.6	13.6	89	1032.4
14.6–17.2	15.9	75	1020
17.2–19.8	18.5	43	705.2
19.8–22.8	21.3	19	351.5
22.8–25.2	24	13	276.9
		$\sum_{1-9} n = 400$	$\sum_{1-9} nd = 4748.82$

2.2.4. In vitro release studies

To avoid oxidative destruction, 100 mg of each produced microparticle was put in synthetic dialysis bags and submerged in 100 mL phosphate buffer solution pH = 7.2 containing 200 µg/mL ascorbic acid as an antioxidant, followed by fixation in sterilized beakers. Each beaker was put in a shaker bath for 72 h at a rate of 100 cycles per minute at 37 degrees Celsius. At regular intervals, a 3 ml aliquot of the dissolving fluid was taken and replaced with new dissolution fluid (to preserve sink conditions). Using a UV-spectrophotometer, the samples were examined spectrophotometrically at λ_{max} 475 nm to measure the dissolved RIF concentration (content RIF). All of the experimental units ($n = 3$) were examined in triplicate.

2.2.5. Study of the kinetics of release from prepared microparticles

Kinetic patterns of RIF release from microparticles prepared according to equations were studied: zero-order, first order, Higuchi equation and Kors–Meyer–Peppa's equation (Ramteke et al., 2014).

2.2.6. Biological part

The biological part included estimating the anti-bacterial of the polymeric formulations loaded with RIF against Gram-

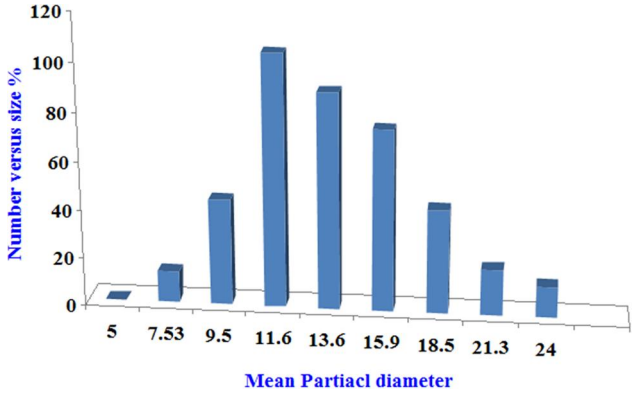

Figure 4. Curve of the distribution of dimensions of RIF micro particles prepared according to the RM1 formulation.

Table 3. Diameters of microparticles estimated in microns and the number of microparticles corresponding to each average dimension for different polymers concentration.

Particle diameter (μm)	Mean particle diameter (μm) d	Number of fields examined (*n*)			
		RM2	RM3	RM4	RM5
9.2–11.8	10.5	0	0	0	0
11.8–13.8	12.8	19	15	8	4
13.8–15.2	14.5	36	21	10	10
15.2–20.8	18	67	26	14	11
20.8–25.2	23	79	47	38	17
25.2–29.8	27.5	90	65	55	43
29.8–32.8	31.3	52	84	89	66
32.8–38.2	35.5	36	65	99	92
38.2–42.8	40.5	11	42	42	99
42.8–48.8	45.8	10	23	32	36
48.8–59.2	54	0	12	13	22
$\sum n$		400	400	400	400
$\sum nd$		10072.4	12172.1	13054.7	14145.8

positive bacteria (*Staphylococcus, aureus*,) and gram-negative bacteria *(Escherichia coli)* and comparing it with the activity of RIF against the same isolates bacterial. The mentioned isolates were activated, and then the culture media was incubated at 37 °C. The efficacy was estimated by measuring the diameter of the inhibition zone according to the Bauer method (Jan et al., 2012).

2.2.7. Cytotoxic test

Cytotoxicity of the RIF microparticles and microparticle without RIF were investigated by using human red blood corpuscles (RBCs) in accordance with a methodology previously published (Sparks & Lorsbach, 2017).

3. Results and discussion

3.1 Morphology and size distribution of microparticles

Optical Microscope (Optika Microscope B-290 series) and Leica ICC50 HD Microscope Camera and worlddidacawardv 2010 computer software employed as one of the ways utilized to prove the spherical form of the manufactured microparticles. When compared to a model without a RIF (Blank), it was discovered that raising the RIF concentration increased the rough surface of the microparticles (Figure 2). The morphological properties of the microparticles utilizing SA at concentrations of (30,50) mg at formula (RM1 and RM2),

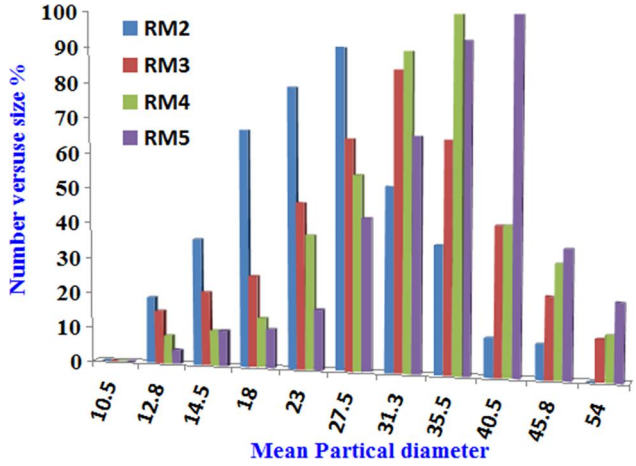

Figure 5. The curve of the distribution of dimensions of RIF microparticles prepared according to the two different polymers concentration.

Table 4. Percentage RIF loading efficiency.

Batch code	Mean particle size (μm)	RIF loading efficiency% ± ($n = 3$)
RM1	11.872	87.32 ± 0.62
RM2	25.181	77.64 ± 0.84
RM3	30.361	71.52 ± 0.37
RM4	32.636	63.94 ± 0.84
RM5	35.3645	54.87 ± 0.93

were round in shape, while when using 75 mg of SA formula (RM3), vesicles with round heads and tapered tails were formed are shown in and Figure 3.

The mean particle size (MPS) of microparticles (400 particles) was determined using an optical microscope with a magnification of (×40) with a calibrated stage micrometer. Table 2 includes the diameters of the prepared microparticles estimated in microns and the number of particles corresponding to each average diameter, and then draws a dimension distribution curve that gives the percentage of the number of microparticles corresponding to each average diameter of dimensions. Table 2 and Figure 4 shows the results of a study of the distribution of diameters of microparticles of RIF drug measured by optical microscopy and prepared according to the formulation RM1 in Table 1 using sodium alginate 30 mg, chitosan 30 mg, and the amount of drug 100 mg. Particle size was calculated by using Eq. (2).

$$\frac{\sum_{1-9} nd}{\sum_{1-9} n} = Mean\ \ particle\ \ diameter \tag{2}$$

According to the data of the above table, the average dimensions of the preparation RM1 are = 11.872 μm

The mean particle size of microparticles of two different polymers concentration are shown in Table 3 and Figure 5. MPS is an important parameter in the evaluation of micro particles, an increase in concentration of SA solution resulted in an increase in size of micro particles. This significant increase may be because of the increase in viscosity of droplets (due to the increase in concentration of SA solution). This increase is high enough to result in difficult dispersal in emulsification and subdivision of droplets. The increase in alginate concentration causes more functional groups to be around the Ca^{+} crosslinking agent and thus additional layers

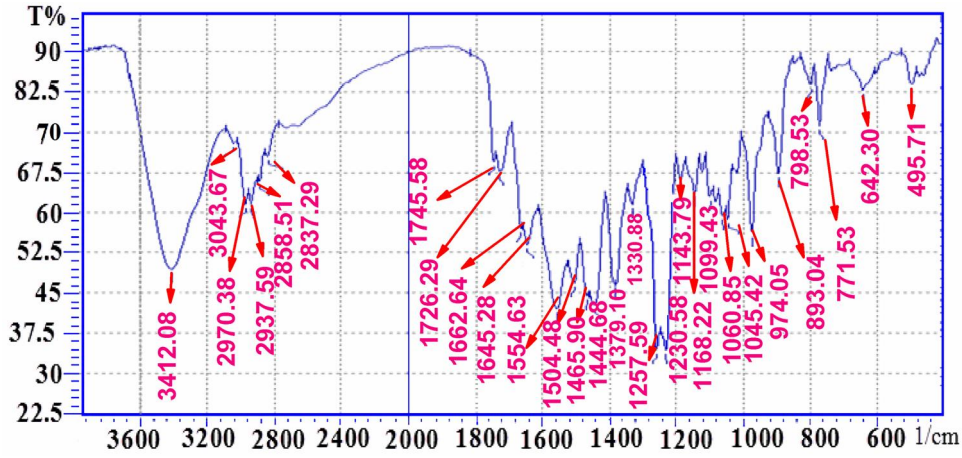

Figure 6. The infrared spectrum of rifampicin.

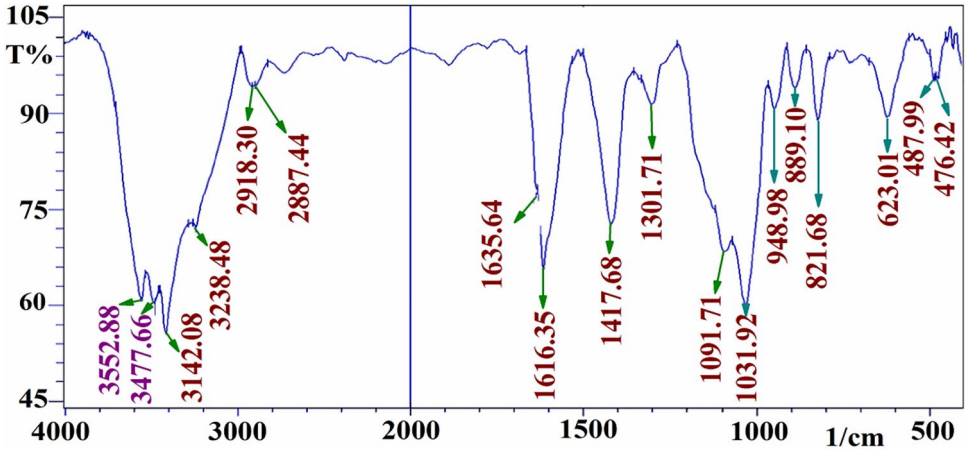

Figure 7. The infrared spectrum of sodium alginate–chitosan microparticles loaded rifampicin.

of alginate chains may join the Ca^{+} cations. This leads to an increase in particle size with the rise in alginate concentration. A similar effect on the external chitosan solution may be attributed to a thicker coat induced by high viscous solution (Formulations RM4, RM5).

The mean particle diameter of the RIF microparticles was 25.181, 30.361, 32.636 and 35.3645 μm for formulations RM2, RM3, RM4 and RM5, respectively.

3.2. RIF drug loading efficiency

The RIF microparticles formulations were subjected to the estimation of drug content. The RIF content was in the range of (54.78% w/w to 87.32% w/w) for the microparticles formulations (as shown in Table 4). The results showed that a smaller drug particle size contribute to a higher RIF loading efficiency%.

3.3. FT-IR spectroscopy

Figures 6–10 show infrared spectra of the prepared microparticles loaded and unloaded with the RIF. Figure 6 illustrates the infrared spectrum of RIF. The spectrum was characterized by the appearance of a peak at (3412.08) cm^{-1} (–NH and –OH stretching) (Sparks & Lorsbach, 2017), 2937.59 cm^{-1} (C–H bonding), 1726.29 cm^{-1} (C = O acetyl stretching), 1662.64 cm^{-1} (C = N stretching), 1645.28 cm^{-1} (C–O–C stretching) 1554.63 cm^{-1} (C = C), 1379.10 cm^{-1} (CH_2, C = C), 1060 cm^{-1} (–CH, CO, C–H), and 974.05 cm^{-1} (≡C–H, C–H). Figure 8 show the infrared spectrum of sodium alginate had characteristic absorption peaks at 3419.79 cm^{-1} (OH stretching), 1627.92 cm^{-1} (carboxylic C = O), 1298 cm^{-1}. The substantial chitosan in peaks showed absorption bands at 3286 cm^{-1}, confirmed NH stretching, 16660 cm^{-1}, confirmed amide (C = O), 1556 cm^{-1}, proclaimed amide (NH) bending, and 1343 cm^{-1}, ascribed to C–N stretching. FT-IR spectrum of the SA/CH microparticles Figure 8, all the characteristic peaks of sodium alginate and chitosan are present, and high-intensity broad bands of hydroxyl stretching and bending at 3419.79 cm^{-1} and 1463 cm^{-1} are observed. This clearly indicates the high intermolecular interactions and formation of hydrogen bonding between the functional groups of both polymers. The peak at 1548 cm^{-1} is the symmetric deformation of ($–NH^{3+}$) resulting from the ionization of primary amino groups in the acidic medium. The peak at 1687 cm^{-1} is characteristic of the carboxylic acid dimmer (due to the acetic acid used for dissolving the chitosan). FTIR study of the SA/CH microparticles loaded with RIF, shown in Figure 7. According to the findings, the RIF spectra exhibited the presence of a number of peaks with distinctive characteristics.

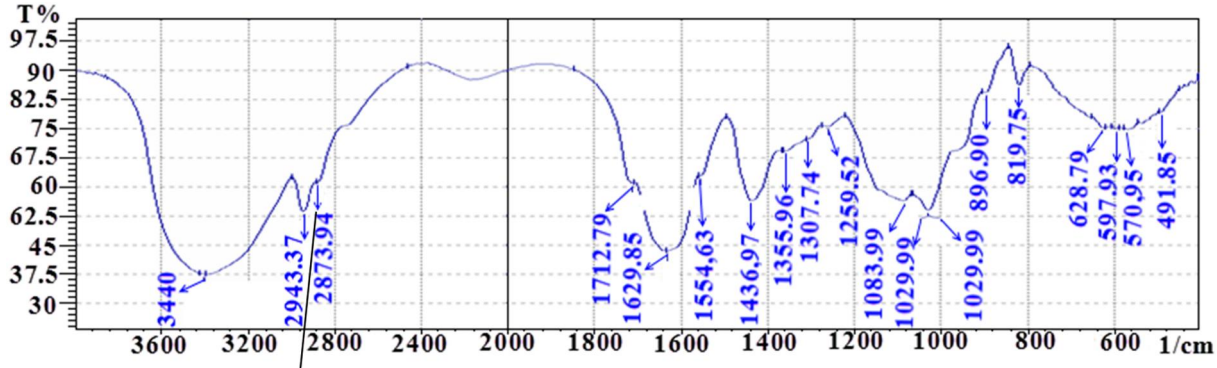

Figure 8

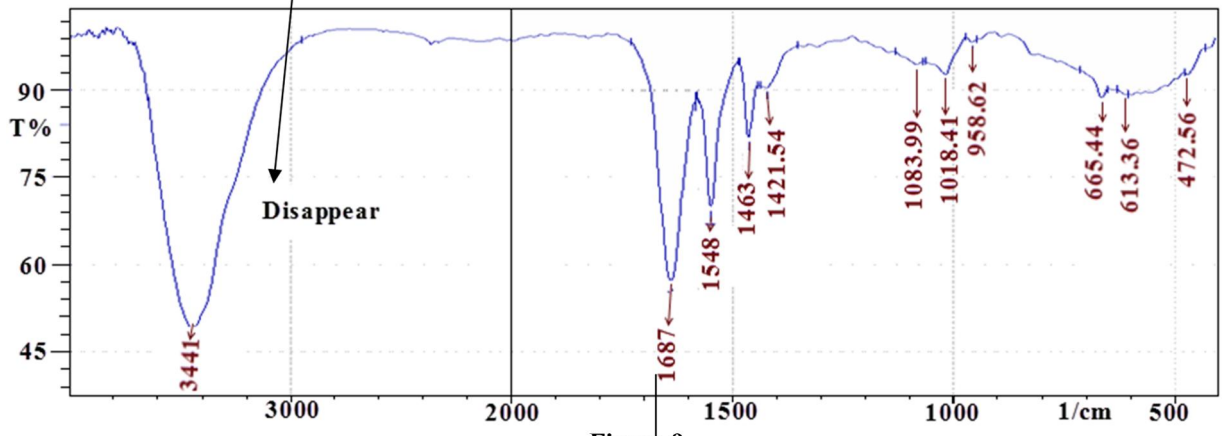

Figure 9

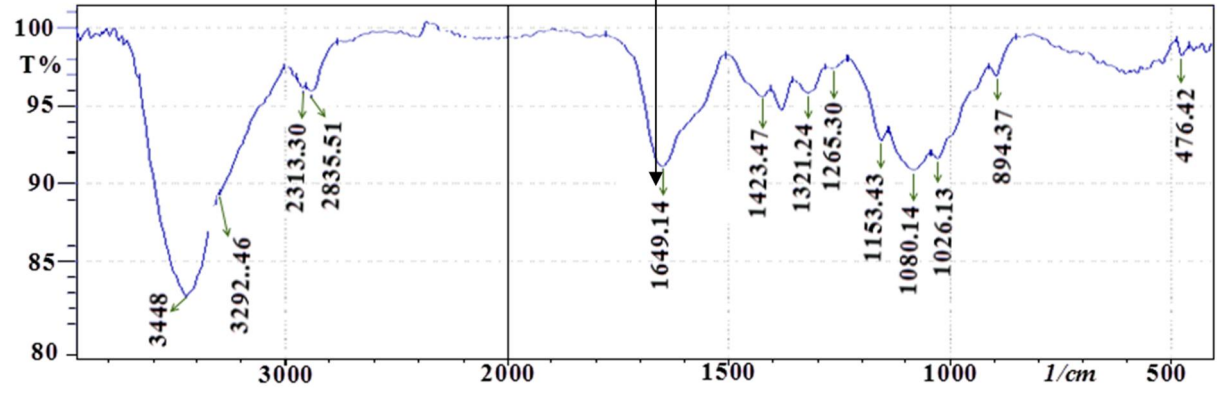

Figure 10

Figures 8–10. The infrared spectrum of sodium alginate (Figure 8). The infrared spectrum of micropartical without RIF (Figure 9), and The chitosan infrared spectrum (Figure 10).

While other peaks changed, this suggests that there was some kind of interaction between the SA/CH microparticles and the RIF drug.

3.4. In vitro release study of RIF

The amount of RIF released by the microparticles must be determined. To prevent oxidative degradation, 100 mg of each manufactured microparticle was placed in synthetic dialysis bags and soaked in 100 mL phosphate buffer solution pH = 7.2 containing 200 μg/mL ascorbic acid as an antioxidant. They were then preserved in sterilized beakers. Each beaker was put in a shaker bath for 72 h at a rate of 100 cycles per minute at 37 degrees celsius. At regular intervals, three millilitres of the dissolving fluid were extracted and replaced with new dissolution fluid. Using a

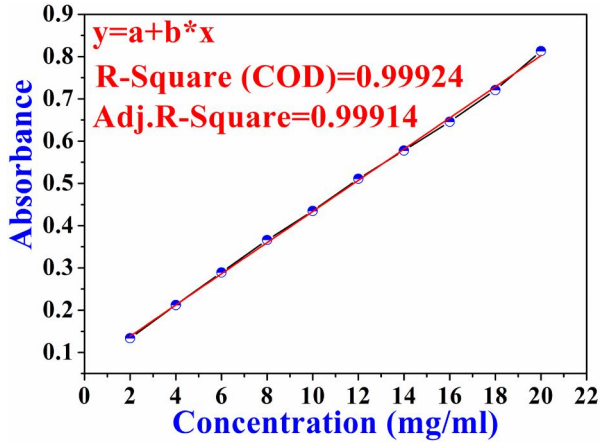

Figure 11. The calibration curve of RIF at pH = 7.2.

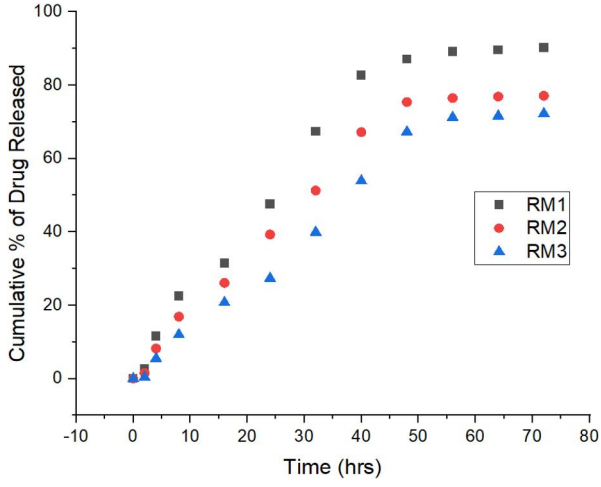

Figure 12. Average percentage RIF release from different SA concentration.

UV-spectrophotometer, the samples were examined spectrophotometrically at λ_{max} 475 nm to measure the dissolved RIF concentration (content RIF). The RIF release was evaluated using the following definitions:

$$\text{Cumulative release } \% = \frac{\text{Amount of drug release (mg)}}{\text{Total amount of drugs loaded}} \times 100\% \quad (3)$$

The calibration of RIF determination is as represented in Figure 11.

Figures 12 and 13 depict the *in vitro* release profiles of various SA/CH concentration microparticle formulations. Because of the reduced particular surface area of formed bigger microparticles, the RIF release rate decreases as the polymer concentration rises. It demonstrates that size is one of the most important factors in controlling microparticle release. Diffusion of a drug (RIF) through a polymer matrix (SA microparticles) is, in principle, dependent on particle size, because the diffusion distance is longer with bigger particles. In addition, dissolution velocity also influenced by the particle size as the specific area increases when particles become smaller. The total RIF liberation was 72.23, 77.1 and

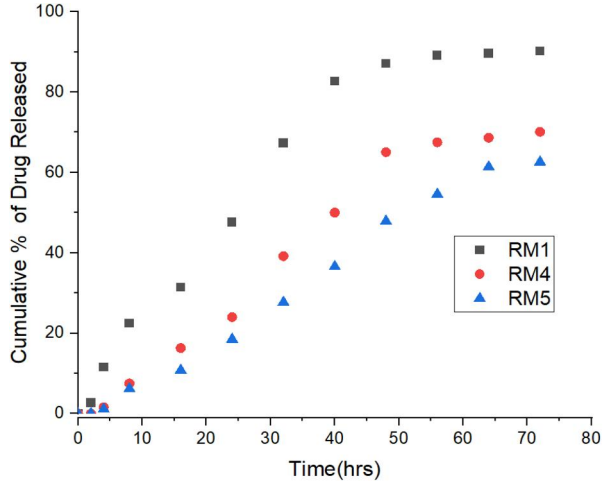

Figure 13. Average percentage RIF release from different chitosan concentration.

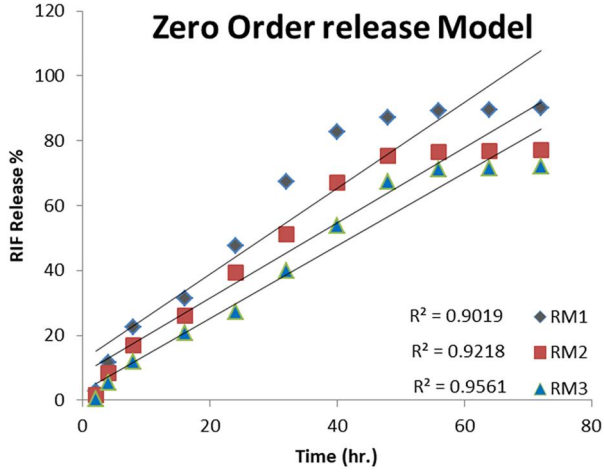

Figure 14. Kinetic of freeing the RIF from the zero order of the microparticles in various concentrations of Sodium alginate.

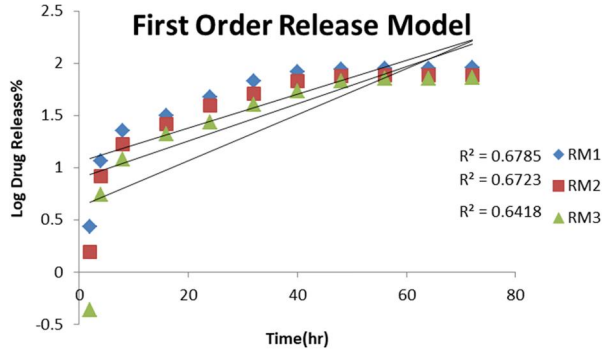

Figure 15. Kinetic of freeing the RIF from the zero order of the microparticles in various concentrations of chitosan.

90.2% after 72 h for 30, 50 and 75 mg sodium alginate concentration, respectively.

3.5. Kinetics of RIF release

Study of the kinetics of release from prepared polymeric microparticles, kinetic patterns of RIF release from microparticles prepared according to equations were studied: zero-order (Figures 14 and 15), First order (Figures 16 and 17),

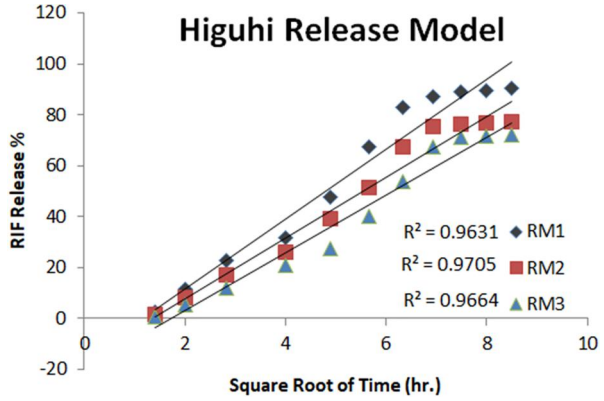

Figure 16. Kinetic of freeing the RIF from the First order of the microparticles in various concentrations of sodium alginate.

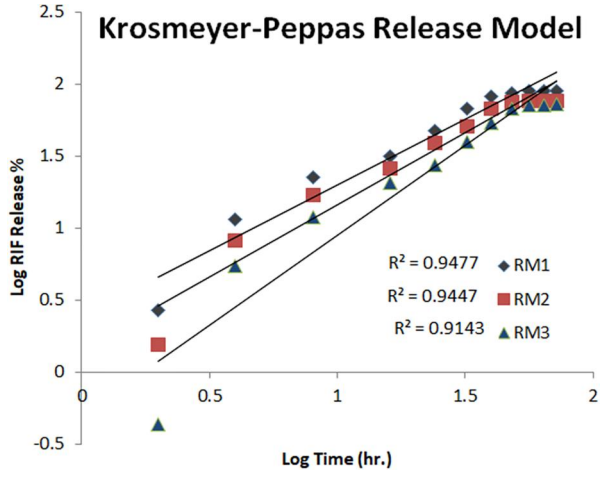

Figure 17. Kinetic of freeing the RIF from the first order of the microparticles in various concentrations of chitosan.

Figure 18. Kinetic of freeing the RIF from the Higuchi equation of the microparticles in various concentrations of sodium alginate.

Higuchi equation (Figures 18 and 19) and Kors–Meyer–Peppa's equation (Figures 20 and 21).

Table 5 lists the slopes as well as the R^2 regression coefficient of determination. The RIF release data was best matched with zero order kinetics (R^2 are $0.9019 - 0.9822$), according to the coefficient of determination, and the Higuchi equation describes the diffusion-controlled release mechanism (Nathanael & Hwan Oh, 2020). Table 5 shows the mechanisms of liberation according to the function (n). Where we notice when ($n \leq 0.45$) the liberation mechanism

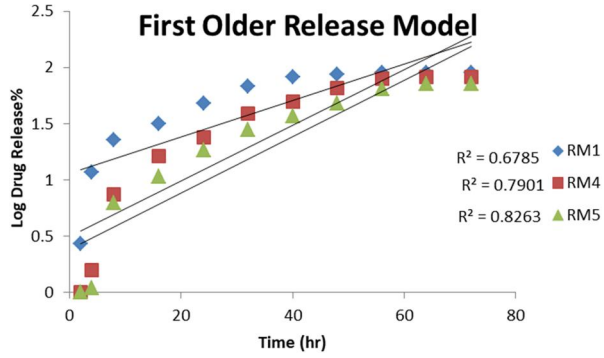

Figure 19. Kinetic of freeing the RIF from the Higuchi equation of the microparticles in various concentrations of chitosan.

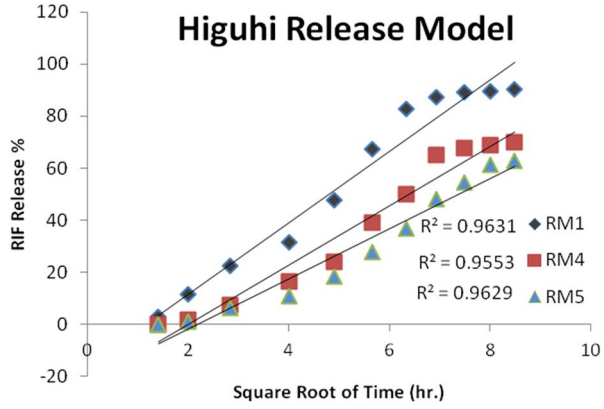

Figure 20. Kinetic of freeing the RIF from the Korsmeyer–Peppa's equation of the microparticles in various concentrations of sodium alginate.

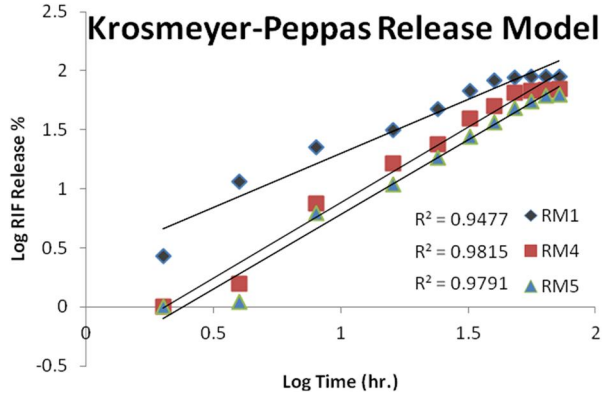

Figure 21. Kinetic of freeing the RIF from the Korsmeyer–Peppa's equation of the microparticles in various concentrations of chitosan.

takes place according to Fickian diffusion mechanism (Motiei et al., 2021; Ramteke et al., 2014) formulations (RM1, RM2, RM3 and RM4) but when it is ($0.45 < n$ formula RM5) this means a release mechanism that is not subject to Fick's law (abnormal release), meaning that the RIF release from the microparticles was controlled by a combination of diffusion and erosion mechanism in addition to the relaxation of polymeric chains.

3.6. Antibacterial efficiency

The antibacterial efficiency was given in Figure 22. The results displayed that effectiveness for the RIF Micro particle

Table 5. Correlation coefficient values for different microparticles formulations.

Formulation	Zero order	First order	Higuchi model	R^2 (Peppas model)	(*n*) Value (Peppa's model)
RM1	0.9019	0.6785	0.9631	0.9477	0.386
RM2	0.9218	0.6723	0.9705	0.9447	0.1606
RM3	0.9561	0.6418	0.9664	0.9143	0.2994
RM4	0.9796	0.7901	0.9553	0.9815	0.4248
RM5	0.9822	0.8263	0.9629	0.9791	0.5082

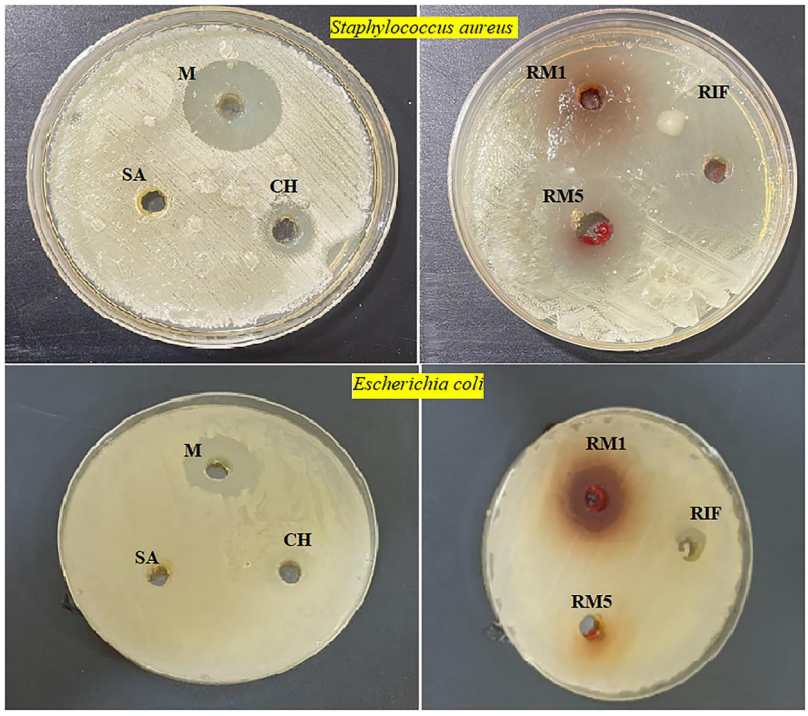

Figure 22. *In vitro* release profile of pure RIF, SA, CH and drug-loaded microparticles: A) The biological activity against *Staphylococcus aureus*. B) The biological activity against *Escherichia coli* at a concentration of 100 mg/ml.

Table 6. The diameter of the inhibition zone (in centimeters) for different microspheres against *Staphylococcus aureus and Escherichia coli*.

Mean diameter of inhibition zone in cm (mean ± SD)*		
Code	*Staphylococcus aureus*	*Escherichia coli*
SA	NZ	NZ
CH	1.0	NZ
M	2.3	1.3
RIF	3.5	0.2
RM1	4.5	2.0
RM5	1.5	0

exceeds effectiveness against clinical isolates *Staphylococcus aurous*, in comparison*with the biological efficiency of RIF alone respectively in inhibiting. This is due to the increase in the biological effectiveness of the SA/CH polyelectrolyte microparticles. Based on the results of well diffusion tests, it was clear that the antibacterial activity of RIF microparticles was substantially more effective against Gram-positive bacteria (*Staphylococcus aurous)* than it was against Gram-negative bacteria (*Escherichia coli*). This impact could be able to be explained by differences in the levels of biological activity shown by different types of bacteria. When compared to Gram-positive bacteria, the structure of the outer membrane

Table 7. Theoretical biological activity of rifampicin.

Pa	Pi	Activity
0.992	0.000	Porphyria
0.994	0.003	Sleep disturbance
0.992	0.001	Hepatitis
0.990	0.000	Torticollis
0.989	0.002	Bronchoconstrictor
0.988	0.002	Asthma
0.987	0.002	Leukopenia
0.987	0.003	Consciousness alteration
0.984	0.001	Agranulocytosis
0.985	0.003	Emetic
0.984	0.003	Xerostomia
0.983	0.002	Thrombocytopenia
0.980	0.003	Nausea
0.977	0.002	Thrombophlebitis
0.976	0.003	Headache
0.976	0.003	Hepatotoxic
0.975	0.003	Dizziness
0.972	0.004	Hematotoxic
0.968	0.004	Sensory disturbance
0.963	0.003	Pain
0.963	0.005	Drowsiness
0.960	0.005	Toxic, gastrointestinal
0.960	0.005	Behavioral disturbance
0.920	0.006	Dyskinesia
0.886	0.013	Toxic
0.811	0.015	Hypertensive

Note: Pa = Pharmacological active, Pi = Pharmacological inactive.

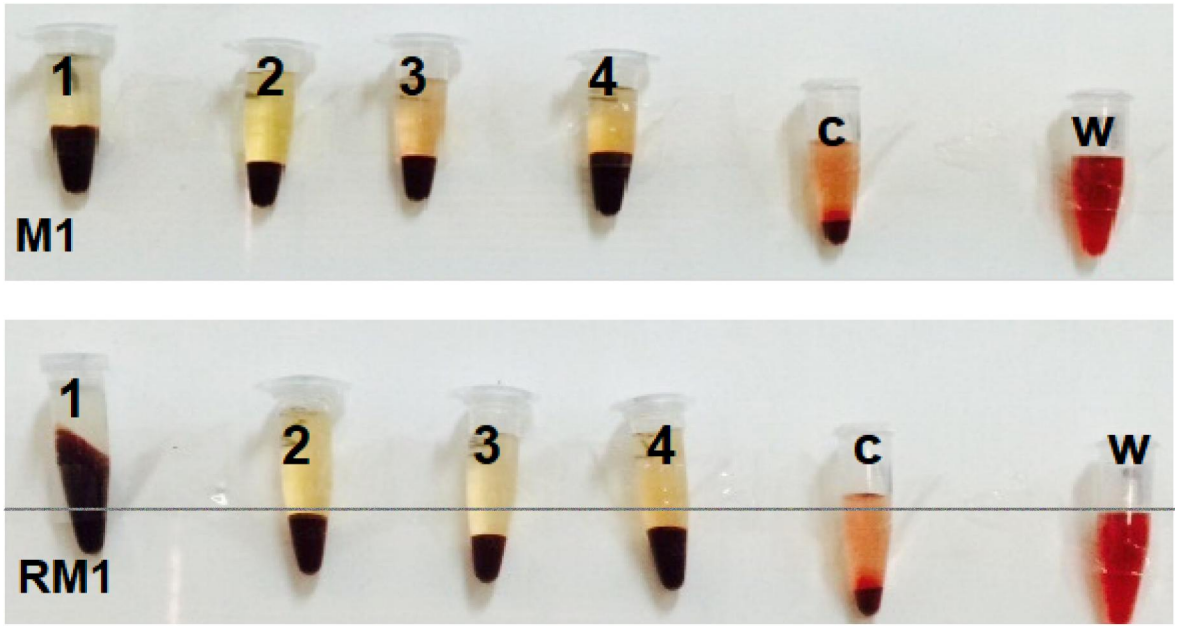

Figure 23. The cytotoxicity of microparticles (M1: sodium alginate/chitosan microparticles without RIF, RM1: RIF micro particle).

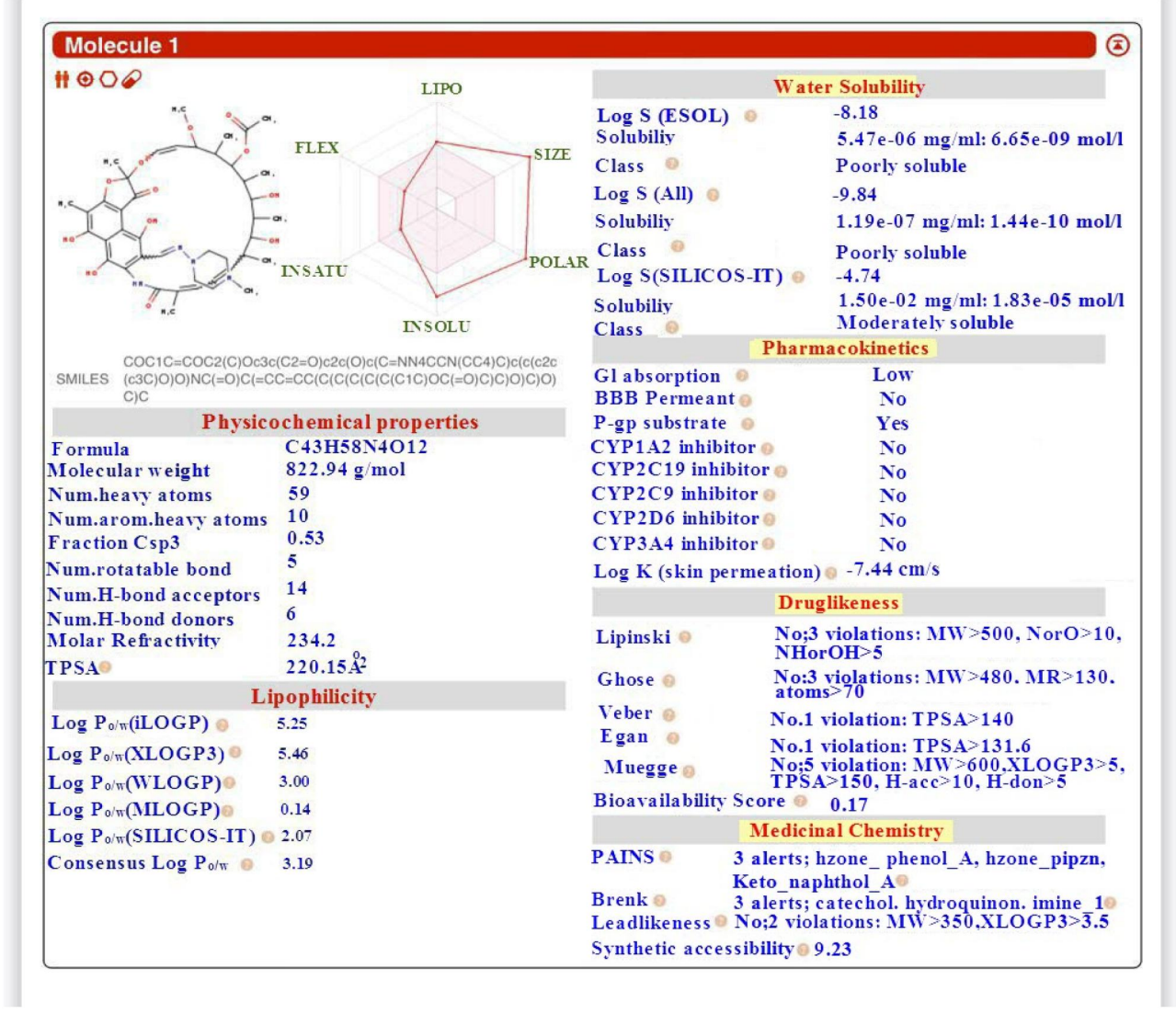

Figure 24. SwissADME results on rifampicin properties. Using the data source SwissADME (http://www.swissadme.ch/index.php/ Swiss Institute of Bioinformatics; accessed on 13 February 2022).

of Gram-negative bacteria produces a barrier that better limits and prevents the entrance of microparticles into the cell. It is possible that variances in the bacterial activity of different species are also connected with the electrostatic interaction between positively charged microparticles and negatively charged bacterial surfaces (Singhvi & Singh, 2011).

The inhibition zone diameters of RIF, sodium alginate, chitosan, SA/CH microparticles (*M*) without RIF and with RIF against two tested bacteria are shown in Table 6. In the current investigation, sodium alginate (SA) did not exhibit any antibacterial activities. On the other hand, the inhibition zone width of chitosan was around one centimeter, suggesting that chitosan shown only moderate antimicrobial activities. SA/CH microparticles (*M*) showed antimicrobial activities against two tested bacteria (*Staphylococcus aureus* and *Escherichia coli*) the inhibition zone diameter was about 2.3 cm and 1.3 cm respectively,

Table 8. The cytotoxicity of the RIF microparticles.

No.	Concentration	M1	RM1
C	Control	NT	NT
1	0.2 μg/ml	NT	NT
2	2 μg/ml	NT	NT
3	20 μg/ml	NT	NT
4	100 μg/ml	NT	NT
W		+	+

*M1: microparticle without RFT, RM1: RIF microparticle control: normal saline, NT: not toxic, + hemolysis occur, w: water.

Table 9. ADMET predicated profile.

Water solubility	−2.924	logS
Plasma protein binding	0.837	100%
Acute oral toxicity	2.255	log (1/(mol/kg))
Tetrahymena pyriformis	0.831	pIGC50 (μg/L)

SA/CH microparticles were prepared by electrostatic interaction between chitosan and sodium alginate, and microparticle antibacterial properties are dependent on the electrostatic interaction of NH_3^+ groups of chitosan and phosphoryl group of lipids on the bacterial cell membrane (Lanctôt et al., 2017) microparticles possess a better antibacterial effect toward Gram-positive than Gram-negative bacteria, due to their cell wall diversity. Peptidoglycan is present in its whole in the cell wall of Gram-positive bacteria (Ana Niurka et al., 2011).

The peptidoglycan layer is made up of networks, and those networks include holes, which make it easy for foreign molecules to enter the cell. On the other hand, Gram-negative bacteria have a cell wall that is made up of a thin membrane of peptidoglycan and an outer membrane that is made up of lipopolysaccharide, lipoprotein, and phospholipids. Due to the bilayer nature of the outer membrane, it provides an effective barrier against foreign molecules that are not native to the cell (Helander et al., 2001). The inhibition zone diameter of pure RIF was 3.5 cm, which was consistent with previous report (Scolari et al., 2020). The inhibition zone diameter of RIF microparticles was 4.5 ± 0.206 cm. Based on these observations, it seems that the antibacterial activity of RIF microparticles is much higher than that of RIF itself. Our findings are in line with those that have been published in the past by a number of other studies. These results might be construed as follows: (1) the effect of the continuous release of microparticles made the microparticles a continuous inhibition of the test bacteria. (2), RIF encapsulation provides effective protection from negative effects and facilitates the antibacterial performance of RIF. The MR1 formulation showed more antibacterial activity than the MR5 formulation since the amount of drug released from MR1 was more

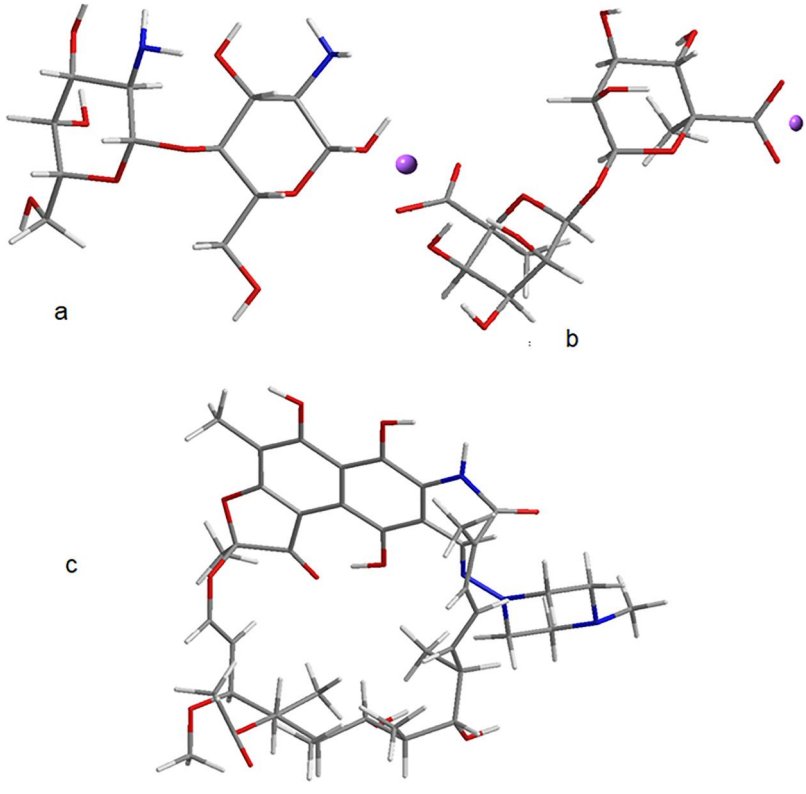

Figure 25. Optimized molecular structure using with DFT model. a) Chitosan (CH), b) sodium alginate (SA) and c) rifampicin (RIF).

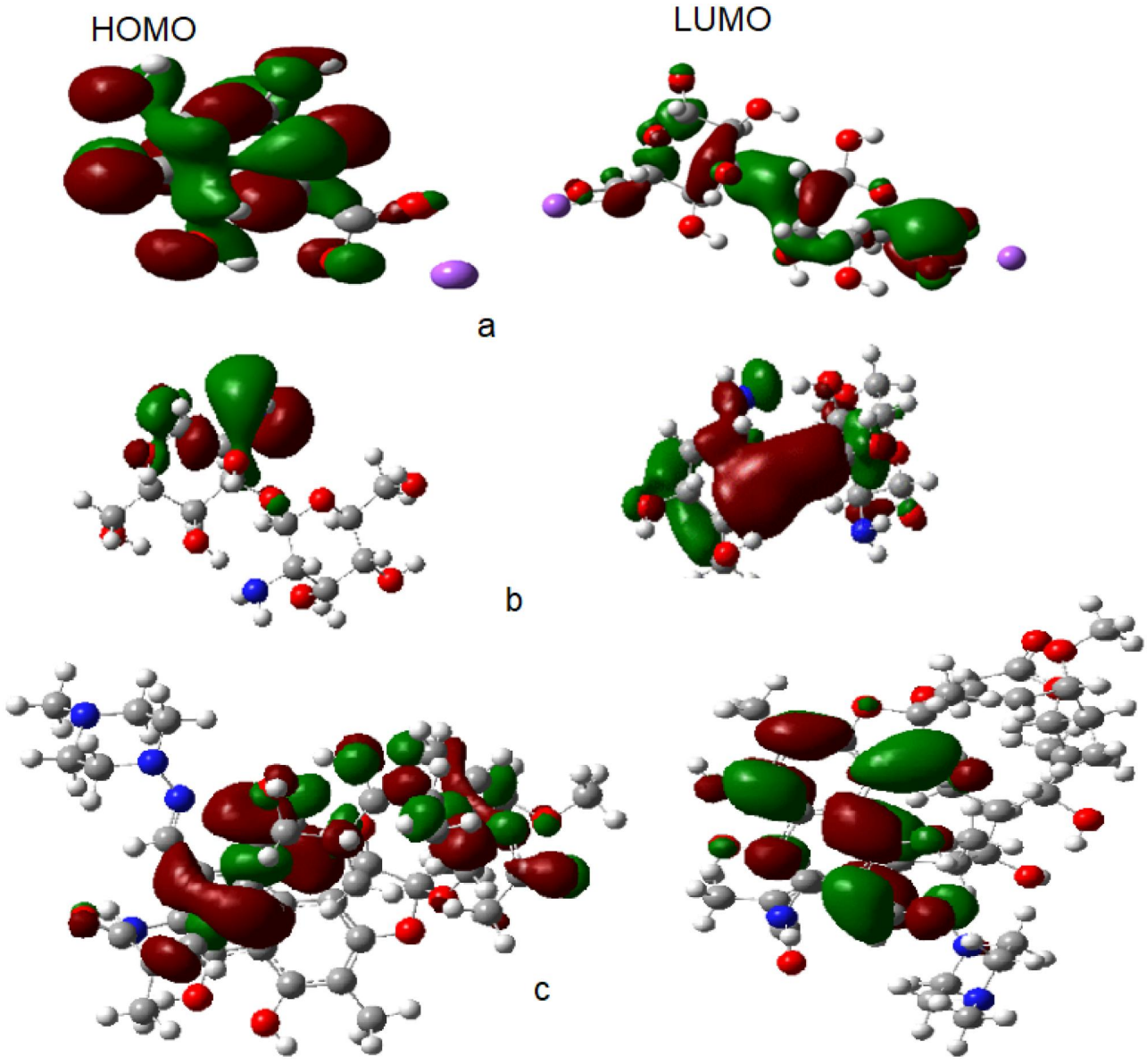

Figure 26. Charge distribution of the HOMO and LUMO orbital for optimized calculated at: (a) B3LYP/(6–311) G (d,p) for sodium alginate, (b) chitosan and (c) rifampicin.

dependent on particle size and RIF Loading Efficiency (Table 4) allowing for better coverage against bacteria.

3.7. Theoretical activity study using a program (avail PASS online free software)

To obtain an expected biological activity profile for the RIF drug, the structural formula of RIF was drawn using the chemoffice15 and PASS Online computer program; to get more information about the biological potential of the RIF drug. The biological activity is shown in Table 7.

3.8. The cytotoxicity of the microparticles

Blood compatibility (Hemocompatibility), is an important evaluation that has to be done with drug delivery systems intended for intravenous administration, as interaction and destruction of blood components result in cellular and humoral reactions that can lead to unwanted inflammation, formation of thrombus, and/or clearance of the drug delivery system from the bloodstream and consequent reduction of drug delivery to the target site, and, thus, reduction of the efficacy of the treatment. Determination of hemocompatibility includes the assessment of hemolysis, protein adsorption on the surface of the particulates, thrombogenicity, and complement activation. The ideal intravenous carrier should be non-hemolytic, non-thrombogenic, non-complement activating, and invisible to the immune system. The hemolysis (red blood cells lysis), and subsequent leakage of free hemoglobin were assessed to estimate the toxicity of the RIF microparticles to human red blood cells.

The results in Table 8 and Figure 23 show the cytotoxicity for RIF microparticles. The human red blood cells within a concentration ranging from (0.2–100) μg/ml for each compound. There was no change in the shape or appearance of the blood after 15, 30, or 60 min of evolution, which

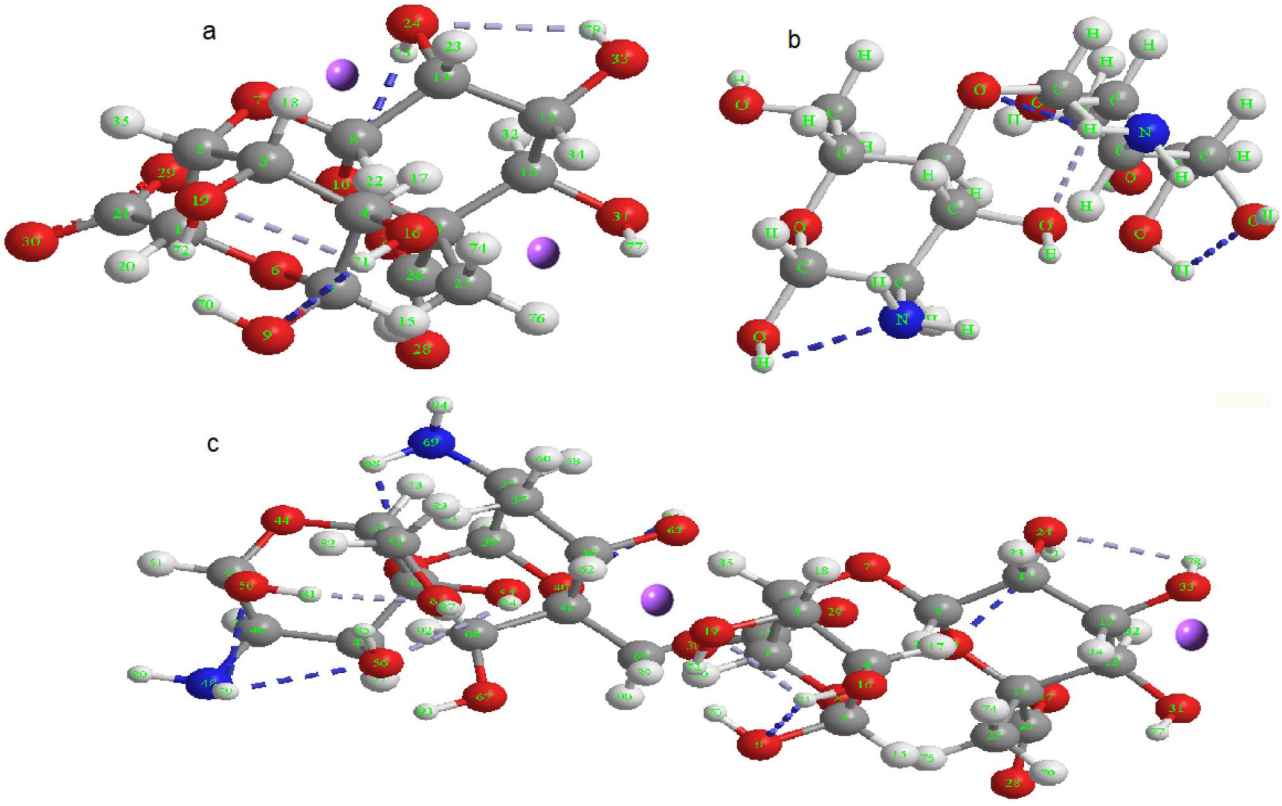

Figure 27. Preferential geometry of the isolated species and the intermolecular H-bonds: (a) MM alginate dimer, (b) protonated chitosan dimer and (c) SA/CH PE interaction, white for hydrogen, gray for carbon, red for oxygen, blue for nitrogen and purple for sodium.

indicates that the prepared RIF microparticles do not have the characteristics of sedimentation or decomposition of human blood cells. The reason for this may be because the prepared RIF microparticles do not have the characteristics of sedimentation or decomposition of human blood cells. The results of the cytotoxicity of the prepared RIF microparticles showed that there was no change in the physiological blood solution and in all the prepared.

3.9. Theoretical cytotoxicity study

The physicochemical characteristics of the RIF medication were subjected to our computational and analytic scrutiny. The most significant components of the physicochemical attributes are broken down into their component parts and summarized in Figure 24 and Table 9. It is essential to point out that the majority of these computations coming from the various platforms may have only minute differences ($< \pm 0.5$) for the same attribute. These properties are mostly focused on the structural features (compound name, structure, molecular formula, MW, TNA, HBA, HBD, RB, PSA and Cm). We used (SwissADME (http://www.swissadme.ch/index.php/) to theoretically analyzed the physicochemical properties.

4. DFT theoretical study

Beginning with the dimer structures of alginate and Chitosan polysaccharides, the purpose of this theoretical work is to examine the probable interactions that stabilize the development of the SA/CS complex. This will be done by starting with dimeric structures. To consider physical, chemical and biological properties of different macromolecules molecular modeling with different level of theories measured as the best choice for such studies (Costa Marcia et al., 2018; Mudeer et al., 2021; Sandeep et al., 2019; Vreven et al., 2001). Molecular modeling at DFT levels were utilized to consider the electronic properties of SA/CHPE. Based on this work further enhancement in the electronic properties of SA/CHPE is achieved as RIF is introduced. Accordingly, this work is conducted to calculate the difference between the highest and the lowest molecular orbital HOMO/LUMO band gap energy at B3LYP/6-311G (d,p) level.

Furthermore, sodium alginate, chitosan, RIF and sodium SA/CH PE also optimized and their HOMO-LUMO band gap energy also were calculated at B3LYP as shown in Figures 25 and 26, respectively. Change in HOMO-LUMO band gap energy ΔE and total dipole moment TDM for sodium alginate. For sodium alginate with CH TDM changed from 13.1335 to 19.2395 Debye and ΔE changed from 1.0368 to 0.7029 eV. Also, HOMO-LUMO band gap energy ΔE and TDM for sodium alginate with RIF were changed to 0.9445 and 0.7029 eV and to 13.1335 and 18.2395 Debye respectively. The intermolecular H-bonds between functional groups of MM alginate dimer and CH dimer is shown in Figure 23 which involves the chitosan amino group NH_3+ and the alginate carboxyl group COO–.

The basic electronic parameters connected to the orbitals in SA/CH PE are the HOMO and LUMO (energy) of (fraction of polymer) can give us an idea about the ground and

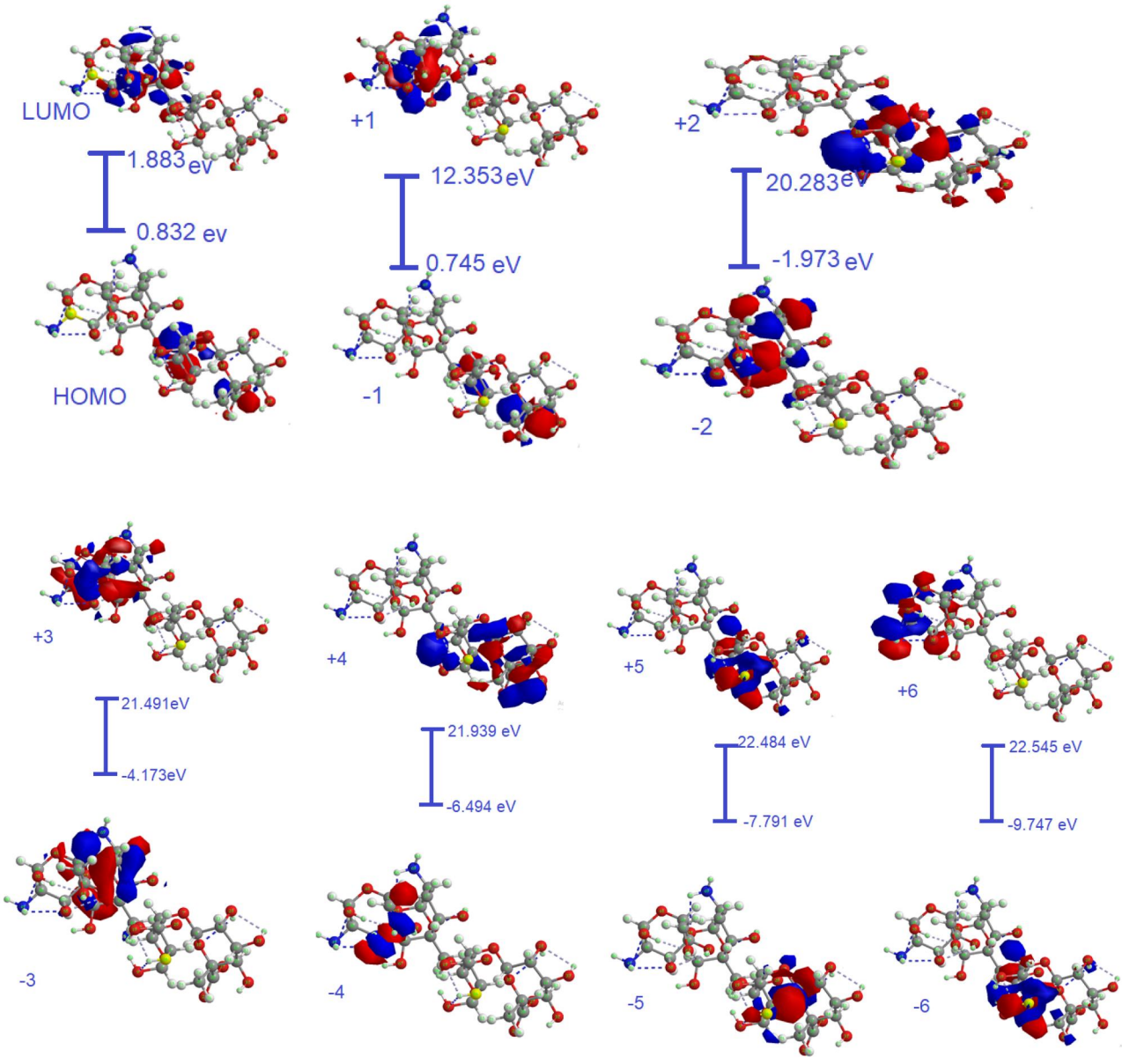

Figure 28. HOMO and LUMO energy for sodium alginate/chitosan (interaction of polymer) using PM3 method.

excited state proton transfer processes. The interaction between the donor and acceptor is characteristic of an electronic absorption band with low energy. One of these molecular complexes is π, the π-complex between neutral molecules. Figures 27 and 28 show the structure proposed of the fraction of polymer (SA/CH interaction of polymer) using PM3 method.

5. Conclusion

Covering the sodium alginate microparticles with chitosan delayed the RIF release by forming a SA/CH polyelectrolyte. The microparticles prepared using 30 and 50 mg sodium alginate in formulation (RM1 and RM2) were round in shape while microparticles prepared using 75 mg sodium alginate formula RM3 included microparticles having rounded heads and tapered tails. The increase in sodium alginate and chitosan concentration affected the particle size, RIF loading efficiency, and RIF release rate. The results showed that smaller drug particle size contributed to higher drug loading efficiency. The data revealed that the microparticles with the higher cumulative release provided by microparticles were Formula RM1 compared to Formula RM5 which had a higher percentage of chitosan. Increasing the sodium alginate and chitosan concentration decreased the RIF release. Sodium alginate microparticles coated with chitosan followed zero-order release kinetics. SA/CH microparticles loaded with RIF have great inhibition effectiveness in comparison to RIF alone against G + ve and G-ve bacteria. *In vitro* studies are an important step in the development of a drug or medical device. They provide the initial evidence that a product is safe and effective, but they cannot replace the need for *in vivo* studies. *In vivo* studies are necessary to evaluate the safety and efficacy of this product. *In vitro* data showed the prepared microparticles to be the stable, safe, small, highly sustainable, and bioactive compared with RIF alone. *In vivo*

studies have yet to be performed, but based on the *in vitro* results obtained, these particles can a beneficial and promising new form of treatment for lung diseases. These particles can inject directly into the lungs and can be used to treat a variety of conditions, including tuberculosis.

The electronic characteristics of SA and CH were investigated using DFT and PM3 principles. The electrostatic potential, total dipole moment TDM, and HOMO/LUMO band gap energy were investigated. TDM of SA and CH were both elevated as a result of the interaction of CH and SA. TDM was raised to 19.2395 Debye for the first likelihood of contact. As a result of the contact, the band gap energy was reduced to 0.7029 eV. The greatest TDM was 12.2080 Debye for the dimer SA interacted with dimer CH across the middle COO^- and NH_3^+ group for the second likelihood of contact. In this situation, however, the lowest value of HOMO/LUMO band gap energy was 0.832 eV.

Compliance with ethical standards

Disclosure statement

The authors declare that they have no conflict of interest.

Ethical approval

Not Applicable

Informed consent

Not applicable.

Funding

The author(s) reported there is no funding associated with the work featured in this article.

References

Atif, S., Haliza, K., & Noraziah, M. Z. (2014). Antibacterial effects of chitosan-tripolyphosphate nanoparticles: Impact of particle size molecular weight. *Journal of Nanoparticle Research*, *16*(7), 2517. https://doi.org/10.1007/s11051-014-2517-9

Ana Niurka, H. L., Miguel Gerardo, V. V., & María Guadalupe, G. S. (2011). Current status of action mode and effect of chitosan against phytopathogens fungi. *African Journal of Microbiology Research*, *5*(25), 4243–4247. https://doi.org/10.5897/AJMR11.104

Buriuli, M., & Verma, D. (2017). Polyelectrolyte complexes (PECs) for biomedical applications, advances in biomaterials for biomedical applications. *Advances in Structural Materials*, *66*, 45–93. https://www.semanticscholar.org

Bazyari, D. S., Badalkhani, K. F., Ebrahim, H. A., & Hadipour, N. L. (2020). Investigation of host–guest interactions between polyester dendrimers and ibuprofen using density functional theory (DFT). *Computational & Theoretical Chemistry*, *1189*, 112983. https://doi.org/10.1016/j.comptc.2020.112983

Bazyari, D. S., Badalkhani, K. F., Ebrahim, H. A., & Hadipour, N. L. (2021). PAMAM and polyester dendrimers as favipiravir nanocarriers: A comparative study using DFT method. *Journal of Nanoparticle Research*, *23*, 231.

Bai, L., Yan, H., Bai, T., Feng, Y., Zhao, Y., Ji, Y., Feng, W., Lu, T., & Nie, Y. (2019). High fluorescent hyperbranched polysiloxane containing β-cyclodextrin for cell imaging and drug delivery. *Biomacromolecules*, *20*(11), 4230–4240. https://doi.org/10.1021/acs.biomac.9b01217

Costa Marcia, P. M., Prates Letícia, M., Leonardo, B., Cruz Maurício, T. M., & Ferreira Ivana, L. M. (2018). Interaction of polyelectrolyte complex between sodium alginate and chitosan dimers with a single glyphosate molecule: A DFT and NBO study. *Carbohydrate Polymers*, *198*, 51–60. https://doi.org/10.1016/j.carbpol.2018.06.052

Fatemeh, N., Mehrab, P., Fatemeh, Y., Keyvan, K., Javad, M., Mohammad, H. S., Faraz, C., Abbas, R., & Francesco, B. (2022). PVA-based nanofibers containing chitosan modified with graphene oxide and carbon quantum dot-doped TiO_2 enhance wound healing in a rat model. *Journal of Functional Biomaterials*, *13*, 300. https://doi.org/10.3390/jfb13040300

Gierszewska, M., Czubenko, J. O., & Chrzanowska, E. (2018). pH-responsive chitosan/alginate polyelectrolyte complex membranes reinforced by tripolyphospha. *European Polymer Journal*, *101*, 282–290. https://doi.org/10.1016/j.eurpolymj.2018.02.031

Hamid, H., Sara, M., Tonelli, A. E., & Hudson, S. M. (2019). Preparation and characterization of chitosan alginate polyelectrolyte complexes loaded with antibacterial thyme oil nanoemulsions. *Applied Sciences*, *9*(18), 3933. https://doi.org/10.3390/app9183933

Hussein Al-Assady, N. A., & Numa, A. K. (2014). *Research Journal of Pharmaceutical Biological & Chemical Sciences*, *5*(4), 295–312. https://www.rjpbcs.com/pdf/2014_5(4)/[31].

Helander, I. M., Nurmiaho, L. E., Ahvenainen, R., Rhoades, J., & Roller, S. (2001). Chitosan disrupts the barrier properties of the outer membrane of Gram negative bacteria. *International Journal of Food Microbiology*, *71*(2–3), 235–244. https://doi.org/10.1016/S0168-1605(01)00609-2

Juarez, M. L. A., Hernandezm, C. H., Chigo, A. E., Aguila, A. E., & Tenorio, M. G. (2017). Chitosan-Aflatoxins B1, M1 interaction: A computational approach. *Current Organic Chemistry*, *21*, 2877–2883. https://doi.org/10.2174/1385272821666170511165159

Jan, S. U., Khan, G. M., Khan, H., Khan, K. A., Shah, S. U., Shah, K. U., Badshah, A., & Hussain, I. (2012). Release pattern of three new polymers in Ketoprofen controlled-release tablets. *African Journal of Pharmacy & Pharmacology*, *6*, 601–607. https://doi.org/10.5897/AJPP11.604

Patra, J. K., Das, G., Fraceto, L. F., Campos, E. V. R., Rodriguez-Torres, M. d P., Acosta-Torres, L. S., Diaz-Torres, L. A., Grillo, R., Swamy, M. K., Sharma, S., Habtemariam, S., & Shin, H.-S. (2018). Nano based drug delivery systems: Recent developments and future prospects. *Journal of Nanobiotechnology*, *16*(17), 2–33. https://doi.org/10.1186/s12951-018-0392-8

Luo, Y., & Wang, Q. (2014). Recent development of chitosan-based polyelectrolyte complexes with natural polysaccharides for drug delivery. *International Journal of Biological Macromolecules*, *64*, 353–367. https://doi.org/10.1016/j.ijbiomac.2013.12.017

Lanctôt, S., Fustier, P., Taherian, A. R., Bisakowski, B., Zhao, X., & Lacasse, P. (2017). Effect of intramammary infusion of chitosan hydrogels at drying-off on bovine mammary gland involution. *Journal of Dairy Science*. *100*(3), 2269–2281. https://doi.org/10.3168/jds.2016-12087

Maryam, R. K., Mehrab, P., Fatemeh, Y., Hamid, R., Mona, N. N., & Bita, R. (2022). Chitosan/agarose/graphitic carbon nitride nanocomposite as an efficient pH-sensitive drug delivery system for anticancer curcumin releasing. *Journal of Drug Delivery Science and Technology, 74*, 103443-103449. https://doi.org/10.1016/j.jddst.2022.103443

Mari, A., Rokstad, A., Lacík, I., Vos, P. d., & Strand, B. L. (2014). Advances in biocompatibility and physico-chemical characterization of microspheres for cell encapsulation. *Advanced Drug Delivery Reviews*, *67-68*, 111–130. https://doi.org/10.1016/j.addr.2013.07.010

Meng, X., Tian, F., Yang, J., He, C.-N., Xing, N., & Li, F. (2010). Chitosan and alginate polyelectrolyte complex membranes and their properties for wound dressing application. *Journal of Materials Science. Materials in Medicine*, *21*(5), 1751–1759. https://doi.org/10.1007/s10856-010-3996-6

Moghimi, R., Ghaderi, L., Rafati, H., Aliahmadi, A., & Julian, D. (2016). McClements, nanoemulsion of thymusdaenensis essential oil against *E. coli*. *Journal of Food Chemistry*, *194*, 410–415. https://doi.org/10.1016/j.foodchem.2015.07.139

Mazini, L., Rochette, L., Hamdan, Y., & Malka, G. (2021). Skin immunomodulation during regeneration: Emerging new targets. *Journal of Personalized Medicine*, *11*(2), 85. https://doi.org/10.3390/jpm11020085

Motiei, M., Pleno de Gouveia, L., Šopík, T., Vícha, R., Škoda, D., Císař, J., Khalili, R., Domincová Bergerová, E., Münster, L., Fei, H., Sedlařík, V., &

Sáha, P. (2021). Nanoparticle-based rifampicin delivery system development. *Molecules*, *26*(7), 2067. https://doi.org/10.3390/molecules26072067

Mudeer, M. M., Fadhela, M. H., & Ramzie, R. A. (2021). Physical properties and biological activity of methyldopa drug carrier cellulose derivatives: *Theoretical study*. *Egyptian Journal of Chemistry*, *64*, 4081–4090. https://ejchem.journals.ekb.eg/article_162496_4cae50f1f30e7cc3eba26b96133b74

Narges, A., Mehrab, P., Fatemeh, Y., Hamid, R., Mona, N. N., Ana, M., & Díez, P. (2022). Chitosan/gamma-alumina/Fe_3O_4@5-FU nanostructures as promising nanocarriers: Physiochemical characterization and toxicity activity. *Molecules*, *27*, 5369. https://doi.org/10.3390/molecules27175369

Narra, K., Dhanalekshmi, U., Rangaraj, G., Raja, D., Senthil Kumar, C., Neelakanta Reddy, P., & Baran Mandal, A. (2012). Effect of formulation variables on rifampicin loaded alginate beads. *Iranian Journal of Pharmaceutical Research*, *11*, 715–721.

Nathanael, A. J., & Hwan Oh, T. (2020). Biopolymer coatings for biomedical applications. *Polymers*, *12*(12), 3061. https://doi.org/10.3390/polym12123061

Patel, N., Lalwani, D., Gollmer, S., Injeti, E., Sari, Y., & Nesamony, J. (2016). Development and evaluation of a calcium alginate based oral ceftriaxone sodium formulation. *Progress in Biomaterials*, *5*, 117–133. https://doi.org/10.1007/s40204-016-0051-9

Pyta, K., Przybylski, P., Klich, K., & Stefańska, J. (2012). A new model of binding of rifampicin and its amino analogues as zwitterions to bacterial RNA polymerase. *Organic & Biomolecular Chemistry*, *10*(41), 8283–8297. https://pubmed.ncbi.nlm.nih.gov/22964663/ https://doi.org/10.1039/c2ob26317c

Ramteke, K. H., Dighe, P. A., Kharat, A. R., & Patil, S. V. (2014). Mathematical models of drug dissolution: A review. *Scholars Academic Journal of Pharmacy*, *3*, 388–396. https://saspublishers.com/media/articles/SAJP35388-396

Sabzini, M., Mehrab, P., Yazdian, F., Khadiv-Parsi, P., & Rashedi, H. (2023). Development of chitosan/halloysite/graphitic-carbon nitride nanovehicle for targeted delivery of quercetin to enhance its limitation in cancer therapy: An *in vitro* cytotoxicity. *International Journal of Biological Macromolecules*, *226*, 159–171. https://doi.org/10.1016/j.ijbiomac.2022.11.189

Sliwoski, G., Kothiwale, S., Meiler, J., & Lowe, E. W. (2014). Computational methods in drug discovery. *Pharmacological Reviews*, *66*(1), 334–395. https://doi.org/10.1124/pr.112.007336

Sohrab, S., Atiyeh, K., Mehrab, P., Fatemeh, Y., Hamid, R., Meisam, O., & Samira, M. (2022). A novel alginate–gelatin microcapsule to enhance bone differentiation of mesenchymal stem cells. *International Journal of Polymeric Materials and Polymeric Biomaterials*, *71*, 395–402. https://doi.org/10.1080/00914037.2020.1848828

Sharma, A., Puri, V., Kumar, P., Singh, I., & Huanbutta, K. (2021). Development and evaluation of rifampicin loaded alginate–gelatin biocomposite microfibers. *Polymers*, *13*(9), 1514. https://doi.org/10.3390/polym13091514

Shariatinia, Z., & Mazloom, J. A. (2019). Chitosan nanocomposite drug delivery systems designed for the ifosfamide anticancer drug using molecular dynamics simulations. *Journal of Molecular Liquids*, *273*, 346–367. https://doi.org/10.1016/j.molliq.2018.10.047

Sparks, T. C., & Lorsbach, B. A. (2017). Agrochemical discovery—building the next generation of insect control agents. In A. D. Gross, Y. Ozoe, J. R. Coats (Eds.), *ACS symposium series* (pp. 12641–17.). American Chemical Society.

Singhvi, G., & Singh, M. (2011). Review: *in-vitro* drug release characterization models. *International Journal of Pharmaceutical Studies & Research*, *2*, 77–84. https://www.technicaljournalsonline.com/ijpsr1

Scolari, I. R., Páez, P. L., Musri, M. M., Petiti, J. P., Torres, A., & Granero, G. E. (2020). Rifampicin loaded in alginate/chitosan nanoparticles as a promising pulmonary carrier against *Staphylococcus aureus*. *Drug Delivery and Translational Research*, *10*(5), 1403–1417. https://doi.org/10.1007/s13346-019-00705-3

Sandeep, K., Monika, N., Neeraj, D., Giovanna, M., Ashraf, A. H., & Ki-Hyun, K. (2019). Nano-based smart pesticide formulations: Emerging opportunities for agriculture. *Journal of Controlled Release*, *294*, 131–153. https://doi.org/10.1016/j.jconrel.2018.12.012

Vos, P., Lazarjani, H. A., Poncelet, D., & Marijke, M. F. (2014). Polymers in cell encapsulation from an enveloped cell perspective. *Advanced Drug Delivery Reviews*, *67–68*, 15–34. https://www.rug.nl/research/pathology/medbiol/pdf/jadvdrugdeliverydevos2014. https://doi.org/10.1016/j.addr.2013.11.005

Vreven, T., Mennucci, B., da Silva, C. O., Morokuma, K., & Tomasi, J. (2001). The ONIOM-PCM method: Combining the hybrid molecular orbital method and the polarizable continuum model for salvation, Application to the geometry and properties of a merocyanine in solution. *The Journal of Chemical Physics*, *115*(1), 62–72. https://aip.scitation.org/doi/abs/10.1063/1.1376127 https://doi.org/10.1063/1.1376127